引用格式：ZHANG Tong, SHI Qiaoya, FENG Ye, et al. Fully Integrated Kerr-lens Mode-locked Ceramic Laser for Low-noise Clock (Invited)[J]. Acta Photonica Sinica, 2025, 54(2):0254103
张彤,史巧雅,冯野,等.面向低噪时钟的全集成克尔透镜锁模陶瓷激光器(特邀)[J].光子学报,2025,54(2):0254103

面向低噪时钟的全集成克尔透镜锁模陶瓷激光器(特邀)

张彤[1,2],史巧雅[1,2],冯野[1,2],王晨[1,2],王屹山[1,2],马彩文[1,2]
(1 中国科学院西安光学精密机械研究所,西安 710119)
(2 中国科学院大学,北京 100094)

摘 要:基于耐辐照的Yb:Y_2O_3陶瓷完成了面向低噪时钟的全集成克尔透镜锁模陶瓷激光器的探索。激光器的中心波长位于1 076.5 nm,光谱宽度为8.58 nm,正常工作状态下,仅需约4 W的功耗即可维持稳定的锁模状态。泵浦结构的优化促使全部光学元件集成于面积为34 mm×78 mm的氮化铝基板上。紧凑的光学结构便于激光器的温度控制,在温控模块的辅助下,激光器连续自由运行2 h的相对功率稳定性可以抑制在0.4%以内。小体积,低噪声,低功耗,使用寿命长的特性使集成化陶瓷激光器有望成为未来引力波探测的理想工具。

关键词:集成光学;固态;超快激光器;克尔效应;天文光学
中图分类号:TN248.1 **文献标识码**:A **doi**:10.3788/gzxb20255402.0254103

0 引言

星系中心的超大质量黑洞及其宿主星系的演化问题一直困扰着众多研究人员。0.1 mHz至1 Hz频段内的引力波辐射源,作为揭示这一谜题的重要线索,已经成为天体物理领域的研究热点。受到地面环境和空间限制的影响,地基探测器难以有效探测该频段的引力波,为此,激光干涉空间天线(Laser Interferometer Space Antenna,LISA),天琴计划和太极计划等星载引力波探测器应运而生[1-3]。三颗全同卫星组成一个臂长10^8～10^9 m的等边三角形,每颗卫星配置两个自由悬浮的检验质量块,通过激光干涉感知并测量相邻卫星质量块之间的相对位移,在高精度时钟的帮助下,实现低频引力波信号的提取[4]。

宇宙空间中的引力波通常仅能引起约10^{-21}量级的空间变化,为满足引力波探测的需求,检验质量块的位移测量精度需达到十皮米量级。同时,星系轨道游离也对激光源频率噪声抑制提出了更高的要求,这些对研究人员而言无疑是一项巨大的挑战。目前,除了利用Pound-Drever-Hall(PDH)稳频[5]和锁臂技术[6]优化干涉仪结构之外,研究人员还采用时间延迟干涉(Time Delay Interferometer,TDI)技术[7-8]来提高引力波的探测精度。TDI技术的本质是对实验获得的相位信息进行时间延迟和线性组合来消除激光源噪声。相位测量的过程中,系统的时钟稳定性要达到10^{-15}量级才能满足引力波探测的需求。该要求对星载原子钟来说并非难题,但体积庞大,结构复杂的特性让研究人员对其望而却步。相较之下,星载石英钟虽然解决了结构和体积等问题,但较低的频率稳定度无疑进一步增加了引力波信号提取的难度。在此情况下,如何提高时钟稳定性并兼顾体积与结构的优化,成为当前亟待解决的关键问题。

2015年,TINTO M等提出了基于光学频率梳的TDI技术[9],即利用光学频率梳极宽的光谱特性,以光学频率梳的重频信号作为外差相位测量的时钟,将激光束相位波动相干地转移到外差测量中使用的微波信

基金项目:国家重点研究发展计划(No. 2022YFC2203804),国家自然科学基金(No. 62435014)
第一作者:张彤, zhangtong@opt.cn
通讯作者:王晨, wangchen@opt.ac.cn;马彩文, cwma@opt.ac.cn
收稿日期:2025-01-24;**录用日期**:2025-02-13
http://www.photon.ac.cn

号上，如此一来便可直接消除激光噪声，极大地简化了系统结构并降低了子系统故障概率。在该技术的驱动下，星载锁模激光器也得到了迅猛发展[10-12]。与光纤星载锁模激光器相比，固体星载锁模激光器在光束质量和寿命方面都更胜一筹。随着激光材料技术的不断进步，掺镱倍半氧化物陶瓷凭借其优异的光学特性、宽广的荧光光谱、高导热性、低声子能量和低量子缺陷，逐渐成为理想的激光增益材料[13-14]。其中，Y_2O_3陶瓷由于具备卓越的抗辐射性和抗损伤性，已成为深空探测领域的理想选择。早在2003年，日本就开始探索基于该材料的被动锁模激光器[15-17]。2021年，FENG Y将基于Y_2O_3陶瓷的1.5 GHz锁模激光器固化于铝基板上，排除了光学调整架为激光器带来的机械漂移，使激光器重复频率的温度敏感度降低了约60%。这不仅提高了频率控制系统的带宽，还进一步降低了激光器的噪声[18]。2023年，OSTAPENKO H通过自制2:1望远镜的泵浦光路，完成了2.2 GHz的克尔透镜锁模陶瓷激光器的完整固化[19]。然而，现有的工作仅展示了基于Y_2O_3陶瓷的固体锁模激光器的集成化雏形，尚不足以成为面向深空探测低噪时钟的最终解决方案。

为了进一步探索基于Y_2O_3陶瓷的固体锁模激光器在引力波探测应用中的潜力，本文对激光器光路和结构进行优化，完成了2.4 GHz克尔透镜锁模陶瓷激光器的完全集成化。完整的陶瓷激光器的尺寸为100 mm×34 mm×18 mm，体积仅为61 mL，自由运转的状态下，该激光器基频时间抖动仅为28 fs（100 Hz～100 MHz），2 h功率波动小于0.4%。

1　GHz克尔透镜锁模陶瓷激光器的集成

小体积、低功耗是Y_2O_3陶瓷锁模激光器面向低噪时钟应用的基本要求。为了满足该需求，陶瓷锁模激光器采用几何容忍度较大的环形腔搭建。图1为完全集成化的2.4 GHz克尔透镜锁模陶瓷激光器，底板上的铜层用于优化腔镜位置。采用厚度为2 mm的Yb:Y_2O_3陶瓷作为激光器的增益介质，其中Yb离子的掺杂浓度为3.5%。四个腔镜分别由两个曲率半径为15 mm的凹面镜（CM1、CM2）和两个平面镜（M1、M2）构成，CM1背后镀有976 nm的高透膜，用于有效激励腔内增益介质并产生激光。M1后方配置有最大行程为4.6 μm的压电陶瓷，能够实现约88 kHz的重复频率调节范围。作为谐振腔输出镜，M2的透过率为0.2%。为了调节腔内色散并产生孤子脉冲，M2还另外镀有Gires-Tournois interferometers涂层，该涂层可在1 040～1 090 nm波段内提供−550 fs²的色散。

图1　集成的克尔透镜锁模陶瓷激光器
Fig.1　The integrated Kerr-lens mode-locked ceramic laser

由于布儒斯特角入射的光线在谐振腔的切向面和矢状面上存在不同的几何路径，因此，上述环形腔结构中，所有腔镜均需设置12°的折叠角以补偿像散。图2为基于ABCD矩阵的谐振腔稳定性和腔内光斑分析结果。图2(a)为凹面镜和晶体的间距对谐振腔稳定性的影响。当凹面镜和晶体的间距为7.4～8.4 mm时，谐振腔的切向面光束和矢状面光束均处于稳定状态，其中，凹面镜和晶体的间距为7.9 mm时，谐振腔稳定性状态最佳。图2(b)为腔内光斑随位置的变化情况，经线性色散补偿后，切平面和矢状面在增益介质处的光斑尺寸分别为14.26 μm和14.93 μm。

基于上述模拟结果，将中心波长为976 nm，最高输出功率为1 W的商用激光二极管所输出的高斯光束，通过定制的准直器实现高斯光束变换。变换后的束腰半径为8 μm，同时，束腰与准直器输出端面的距离为12 mm。商用激光二极管在准直器后的输出功率和电流之间的关系曲线见图3，斜效率约为65%。束腰处的光束轮廓也如图3所示，椭圆度为98.1%。

连续工作状态下，激光器的温度漂移是不可避免的。与望远镜的泵浦结构相比，定制准直器使激光器

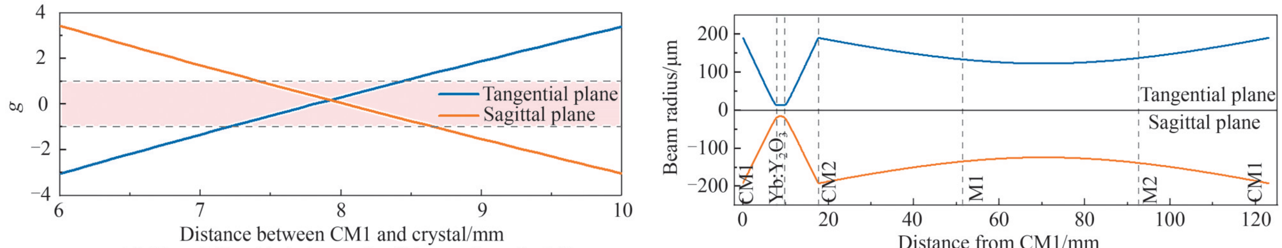

(a) The relationship between the distances from the M1 to the $Yb:Y_2O_3$ and the stability of the resonator

(b) Beam radius within the cavity

图2 2.4 GHz克尔透镜锁模陶瓷激光器的设计

Fig. 2 The design of the 2.4 GHz Kerr-lens mode-locked ceramic laser

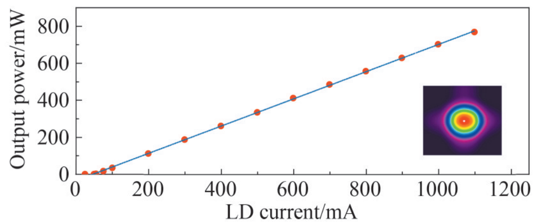

图3 激光二极管在准直器后的输出功率与电流之间的关系。插图：束腰处的光束轮廓

Fig.3 The relationship between the output power and the current of the LD. Inset figure: beam profile of pump laser at the focal plane

结构更加紧凑，更加便于温度控制。作为谐振腔与温度控制模块之间的桥梁，底板材料的选择尤为重要。现有的工作曾尝试采用铝材和熔融石英作为底板[18-20]，但铝材较高的线性膨胀系数和熔融石英的低热导率均可能引起空腔长度大幅波动，从而为激光器的长期稳定性留下隐患。为此，集成化2.4 GHz陶瓷激光器的底板拟尝试一种新材料——氮化铝陶瓷。综合考虑材料的热膨胀、导热性能和强度定义才能更好地评估以上三种材料，基于这些因素，本文定义了激光器底板的品质因数（Figure Of Merits, FOM）为

$$\mathrm{FOM}=\frac{K\times E}{\mathrm{CTE}}$$

式中，K、E、CTE分别表示热导率、杨氏模量和线性膨胀系数，这些固有性质数值见表1。从表1可以看出，与其他两种材料相比，氮化铝陶瓷作为激光器底板的潜力巨大。

表1 铝、熔融石英和氮化铝陶瓷的关键固有物理特性[21]

Table 1 The key inherent physical characteristics in aluminum, fused silica, and AlN ceramic[21]

Material	CTE/K^{-1}	E/Pa	K/(W·(m·K)$^{-1}$)	FOM/(W·Pa·(m·K^2)$^{-1}$)
Aluminium	23.6×10^{-6}	68×10^{9}	237	7.007×10^{17}
Fused silica	5×10^{-7}	73×10^{9}	1.4	2.044×10^{17}
Aluminum nitride	4.2×10^{-6}	33×10^{10}	190	1.49×10^{19}

激光器的温度控制模块由铜块和半导体制冷片（Thermo Electric Cooler, TEC）构成，其体积总和约为50 mL。图4为温度控制模块的波特图。24.4 Hz的温度控制带宽可以减缓大多数热冲击。通常，激光器在设定温度23 ℃的环境下工作，此时TEC所产生的功耗为0.5 W，而其能效可以达到242%。

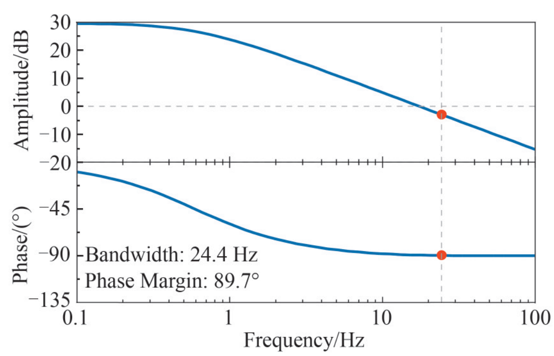

图4 温度控制模块的波特图

Fig.4 The Bode diagram of the temperature control

2 集成激光器的性能和测量结果

优化凹面镜和增益介质之间的距离来增强谐振腔的非线性损耗，激光器便可基于软孔径光阑实现锁模自启

动。锁模达到稳定状态后，将腔镜固化在34 mm×78 mm的氮化铝陶瓷底板上，实现全集成化的克尔透镜锁模陶瓷激光器。集成化的陶瓷激光器能够在泵浦电流达到445 mA时，开启锁模状态。当泵浦电流处于445 mA和545 mA之间时，集成化的陶瓷激光器均工作在锁模状态，此时的谐振腔只允许一个方向工作，其最大输出功率达到15.1 mW。图5为泵浦二极管的电流与激光器输出功率的关系曲线。蓝色曲线表示锁模方向的输出功率，灰色区域为激光器的锁模范围。

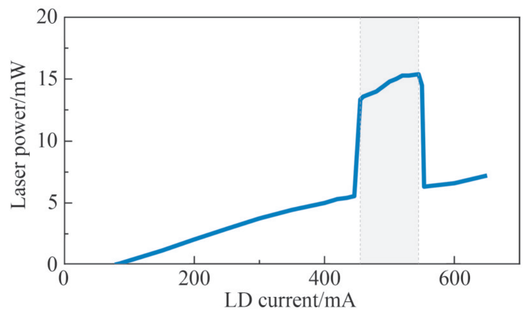

图5　集成化激光器的输出功率与泵浦电流的关系

Fig.5　The relationship between the output optical power and the LD Current.

图6(a)和(b)分别为集成化陶瓷激光器的光谱特性和自相关曲线，当泵浦电流为530 mA时，光谱的中心波长位于1 076.5 nm，3 dB带宽处光谱宽度为8.58 nm，光谱右侧的尖峰主要源于腔内色散分布。双曲正割型的自相关曲线对应151 fs的飞秒脉冲。图7为集成化陶瓷激光器连续工作两小时的相对功率稳定性，红色虚线为线性拟合结果，其斜率为2.13×10^{-6}。0.4%的功率漂移证明了该温度控制模块的优异性能。

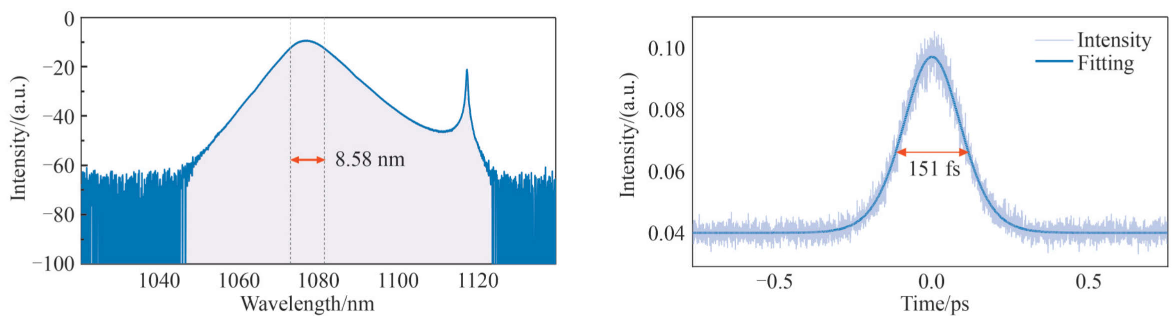

(a) The optical spectrum　　(b) The autocorrelation trace

图6　集成化陶瓷激光器的光学特性

Fig.6　The optical characteristics of the integrated ceramic laser

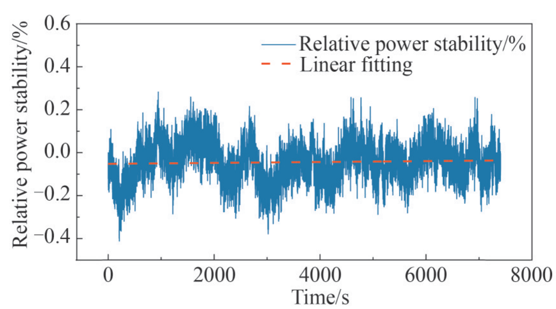

图7　集成化陶瓷激光器的相对功率稳定性

Fig.7　The Relative power stability of the integrated ceramic laser

图8是利用带宽为2.4 GHz的光电探测器，在信号源分析仪（Rohde & Schwarz，FSWP50）上采集到集成化陶瓷激光器的频谱特性。图片右上角为2.439 GHz的基频的局部放大图，其信噪比为86.7 dB。图9中的蓝色曲线描述的是集成化陶瓷激光器在自由运行状态下的相位噪声特性。从图9可以看出，在100 Hz、 1 kHz、10 kHz、100 kHz、1 MHz、10 MHz、100 MHz偏移频率下，激光器的相位噪声（Phase Noise，PN）的功率谱密度分别为−87.45 dBc/Hz，−115.29 dBc/Hz，−138.24 dBc/Hz、−156.12 dBc/Hz、−166.21 dBc/Hz、−167.53 dBc/Hz、−168.45 dBc/Hz。100 Hz到100 MHz的积分时间抖动为28 fs，其中100 Hz到200 Hz的偏移频率所贡献的时间抖动超过了87%，此范围的相位噪声主要来源于仪器设备运行造成的平台振动和气流扰动。

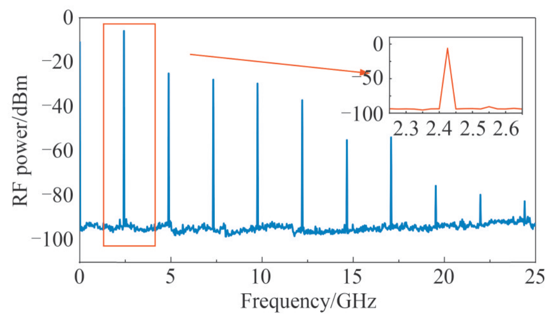

图8　集成化陶瓷激光器的频谱特性

Fig.8　The radio-frequency spectrum of the integrated ceramic laser

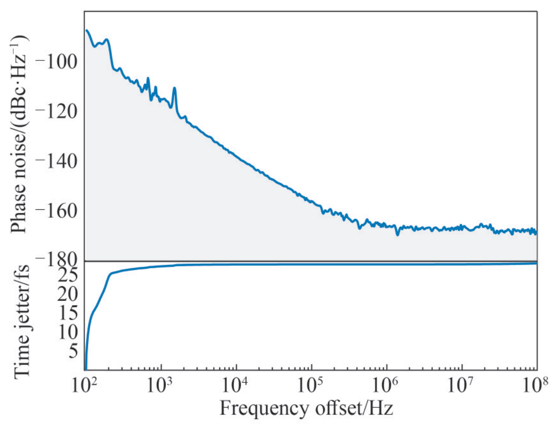

图9　集成化陶瓷激光器的相位噪声特性曲线

Fig.9　The phase noise of the integrated ceramic laser

3　结论

紧凑的结构设计促使克尔透镜锁模激光器实现全集成化。集成化陶瓷激光器的体积为61 mL，仅4 W的功耗便可维持稳定地锁模状态。该激光器的重复频率为2.439 GHz，其中心波长位于1 076.5 nm附近，光谱宽度和脉冲宽度分别为8.58 nm和151 fs。自由运转2 h的情况下，激光器的功率稳定度及定时抖动分别能到达0.4%和28 fs（100 Hz～100 MHz）。得益于Y_2O_3优异的抗辐射性和抗损伤性，小体积、低功耗，低噪声的集成化陶瓷激光器有望成为引力波探测的理想时钟。压电陶瓷的加入能够进一步提高参考时钟的准确度，为提高引力波探测的精度提供坚实的基础。此外，集成化陶瓷激光器在光通讯、精密测量和光学计量等领域也有着广泛的应用前景，是人类探索未知领域的强有力工具。

参考文献

[1] AMARO-SEOANE P, ANDREWS J, ARCA SEDDA M, et al. Astrophysics with the laser interferometer space antenna[J]. Living Reviews in Relativity, 2023, 26(2):1-328.

[2] LUO Jun, CHEN Lisheng, DUAN Huizong, et al. TianQin: a space-borne gravitational wave detector[J]. Classical and Quantum Gravity, 2016, 33(3):035010.

[3] GAO Ruihong, LIU Heshan, LUO Ziren, et al. Introduction of laser pointing scheme in the Taiji program[J]. Chinese Optics, 2019, 12(3):425-431.
郭瑞弘，刘河山，罗子人，等.太极计划激光指向调控方案介绍[J].中国光学, 2019, 12(3):425-431.

[4] XU M, WU H, LIANG Y, et al. Weak-light phase-locking time delay interferometry with optical frequency combs[J]. Sensors, 2022, 22(19):7349.
[5] THORPE J I, NUMATA K, LIVAS J. Laser frequency stabilization and control through offset sideband locking to optical cavities[J]. Optics Express, 2008, 16(20):15980-15990.
[6] WU H, KE J, WANG P P, et al. Arm locking using laser frequency comb[J]. Optics Express, 2022, 30(5):8027-8048.
[7] HELLINGS R W. Elimination of clock jitter noise in spaceborne laser interferometers[J]. Physical Review D, 2001, 64(2): 022002.
[8] TINTO M, ESTABROOK F B, ARMSTRONG J W. Time-delay interferometry for LISA[J]. Physical Review D, 2002, 65(8): 082003.
[9] TINTO M, YU N. Time-delay interferometry with optical frequency comb[J]. Physical Review D, 2015, 92(4): 042002.
[10] WILKEN T, LEZIUS M, HÄNSCH T W, et al. A frequency comb and precision spectroscopy experiment in space[C]. CLEO: 2013.
[11] LEE J, LEE K, JANG Y S, et al. Testing of a femtosecond pulse laser in outer space[J]. Scientific Reports, 2014, 4(1): 5134.
[12] LEZIUS M, WILKEN T, DEUTSCH C, et al. Space-borne frequency comb metrology[J]. Optica, 2016, 3(12): 1381-1387.
[13] KONG J, TANG D Y, LU J, et al. Spectral characteristics of a Yb-doped Y_2O_3 ceramic laser[J]. Applied Physics B, 2004, 79(4):449-455.
[14] SANGHERA J, KIM W, VILLALOBOS G, et al. Ceramic laser materials: past and present[J]. Optical Materials, 2013, 35(4):693-699.
[15] SHIRAKAWA A, TAKAICHI K, YAGI H, et al. Diode-pumped mode-locked Yb^{3+} : Y_2O_3 ceramic laser[J]. Optics Express, 2003, 11(22):2911-2916.
[16] ENDO M, ITO I, KOBAYASHI Y. Direct 15-GHz mode-spacing optical frequency comb with a Kerr-lens mode-locked Yb:Y_2O_3 ceramic laser[J]. Optics Express, 2015, 23(2):1276-1282.
[17] KIMURA S, TANI S, KOBAYASHI Y. Kerr-lens mode locking above a 20 GHz repetition rate[J]. Optica, 2019, 6(5):532-533.
[18] FENG Y, LAMOUR T P, OSTAPENKO H, et al. Towards a space-qualified Kerr-lens mode-locked laser[J]. Optics Letters, 2021, 46(21):5429-5432.
[19] OSTAPENKO H, FENG Y, LAMOUR T, et al. Misalignment-free, Kerr-lens-modelocked Yb: Y_2O_3 2.2-GHz oscillator, amplified by a semiconductor optical amplifier[J]. Optics Express, 2023, 31(2):3249-3257.
[20] DELGOFFE A, NAZIR S, HAKOBYAN S, et al. All-glass miniature GHz repetition rate femtosecond laser cavity[J]. Optica, 2023, 10(10):1269-1279.

Fully Integrated Kerr-lens Mode-locked Ceramic Laser for Low-noise Clock (Invited)

ZHANG Tong[1,2], SHI Qiaoya[1,2], FENG Ye[1,2], WANG Chen[1,2], WANG Yishan[1,2], MA Caiwen[1,2]
(1 *Xi'an Institute of Optics and Precision Mechanics, Chinese Academy of Sciences, Xi'an* 710119, *China*)
(2 *University of Chinese Academy of Sciences, Beijing* 100094, *China*)

Abstract: Detecting Gravitational Waves (GWs) in the 0.1 mHz to 1 Hz range is a crucial step in exploring the longstanding astrophysical mysteries surrounding the coevolution of supermassive black holes at galactic centers and their host galaxies. It is estimated that GWs can only induce spatial changes on the order of 10^{-21}, which poses a significant challenge for ground-based observatories due to spatial constraints and interference from the ground and atmosphere. Fortunately, space-based GWs observatories can offer promising solutions, where signals are expected to be larger in number and characterized by larger amplitudes. Notable examples include the Laser Interferometer Space Antenna (LISA), Tianqin, and Taiji. All these missions deploy three synchronized satellites in a triangular configuration, separated by arm lengths of $10^8 \sim 10^9$ meters, forming a colossal interferometer in space. Each satellite houses two free-falling test masses, whose relative displacements are monitored via laser interferometry. By analyzing the movement between these masses with ultra-stable clocks, scientists aim to extract faint GWs buried in noise. The detection of GWs necessitates displacement measurements with an extraordinary precision of

tens of picometers. Achieving such precision demands the suppression of noise sources, particularly laser frequency fluctuations, to an extraordinary degree. In addition to optimizing the structure of the interferometer using Pound-Drever-Hall (PDH) frequency stabilization and arm-locking techniques, researchers are now using Time-Delay Interferometer (TDI) techniques to improve the accuracy of gravitational wave detection. TDI represents a computational tour de force: it processes phase data collected from satellites at varying light-travel times and combines them algorithmically to cancel laser frequency fluctuations. For example, differential measurements between satellites are delayed and summed to nullify phase drifts caused by imperfect laser coherence. This approach effectively mitigates noise while preserving GW signatures. A critical subsystem is the timing system. To meet the requirements of GWs detection, phase measurements require clock stability better than 10-15. Traditional atomic clocks meet the stability requirements but are impractical for space missions due to their size, weight, and power consumption. In contrast, quartz clocks offer advantages in size and weight but fall short in stability. Under this circumstance, improving the clock's stability while optimizing its size and structure has become a critical challenge to address. The optical frequency comb-based TDI (OFC-TDI) technique was proposed to simplify the difficulty. OFCs generate ultra-stable, evenly spaced spectral lines across a broad frequency range. OFC-TDI technique uses the repetition frequency of the OFC as the clock for the heterodyne measurements, allowing phase fluctuations to be coherently transferred to microwave signals through its broad spectral characteristics. This approach directly eliminates laser noise, significantly simplifying the system structure and reducing the likelihood of subsystem failures. Recent advancements in miniaturizing mode-locked lasers, the core components of OFCs, have accelerated the development of compact, space-qualified systems. Compared to fiber lasers, solid-state lasers provide superior beam quality and longer lifetime. This paper presents an integrated Kerr lens-locked laser based on an irradiation-resistant $Yb:Y_2O_3$ ceramic for the low-noise clock. The laser is fully integrated into a compact volume of 61 mL. By optimizing the pump structure, all optical components of the laser are confined to an area of 34×78 mm^2, which allows for precise temperature control. The temperature control helps the laser achieve a timing jitter of 28 fs. The low power consumption of the laser is only 4 W. The small size, low noise, low power consumption, and long lifetime make the integrated ceramic laser as an ideal tool for gravitational wave detection. In addition, the laser operates near a center wavelength of 1 076.5 nm with a spectral width of 8.58 nm. The relative power stability of the laser is within 0.4% over a two-hour period.

Key words: Integrated optics; Solid-state; Ultrafast lasers; Kerr effect; Astronomical optics

OCIS Codes: 250.4390; 140.3580; 140.7090; 190.3270; 350.1260

CSTR: 32255.14.10.3788/gzxb20255402.0254103

Foundation item: National Key Research and Development Program of China (No. 2022YFC2203804), National Natural Science Foundation of China (No. 62435014)